Neuron
Article

Cellular and Synaptic Architecture of Multisensory Integration in the Mouse Neocortex

Umberto Olcese,[1,2] Giuliano Iurilli,[1,2] and Paolo Medini[1,3,*]
[1]Department of Neuroscience and Brain Technologies, Istituto Italiano di Tecnologia, Via Morego, 30, 16163 Genova, Italy
[2]These authors contributed equally to this work
[3]Present address: Molecular Biology and Integrative Medical Biology (Physiology Section) Departments, Umeå University, 901 87 Umeå, Sweden
*Correspondence: paolo.medini@iit.it
http://dx.doi.org/10.1016/j.neuron.2013.06.010

SUMMARY

Multisensory integration (MI) is crucial for sensory processing, but it is unclear how MI is organized in cortical microcircuits. Whole-cell recordings in a mouse visuotactile area located between primary visual and somatosensory cortices revealed that spike responses were less bimodal than synaptic responses but displayed larger multisensory enhancement. MI was layer and cell type specific, with multisensory enhancement being rare in the major class of inhibitory interneurons and in the output infragranular layers. Optogenetic manipulation of parvalbumin-positive interneuron activity revealed that the scarce MI of interneurons enables MI in neighboring pyramids. Finally, single-cell resolution calcium imaging revealed a gradual merging of modalities: unisensory neurons had higher densities toward the borders of the primary cortices, but were located in unimodal clusters in the middle of the cortical area. These findings reveal the role of different neuronal subcircuits in the synaptic process of MI in the rodent parietal cortex.

INTRODUCTION

Combining inputs from different modalities improves stimulus detection, builds new representations and helps to resolve ambiguities (Stein and Stanford, 2008). Multisensory integration (MI) occurs in the superior colliculus and in some cortical association areas, the degree of MI being dependent on timing, strength and spatial alignment of the stimuli (Stein and Wallace, 1996). A few studies examined the connectivity behind MI, e.g., in different cortical layers (Foxworthy et al., 2013). Cortical inputs are important for MI in the colliculus (Jiang et al., 2001), and GABAergic neurons are involved in cross-modal suppression in a cat multisensory area (Dehner et al., 2004). However, it is not clear how MI is organized within cortical microcircuits, and at the level of synaptic inputs and spike outputs.

In primary sensory areas, stimulus representation is layer (de Kock et al., 2007; Martinez et al., 2005; Sakata and Harris, 2009) and cell type specific, as shown by the different response properties of inhibitory and excitatory cells in primary visual cortex—V1 (Kameyama et al., 2010; Kerlin et al., 2010; Runyan et al., 2010) and primary somatosensory cortex—S1 (Gentet et al., 2010; Gentet et al., 2012). Because the synaptic organization of cortical microcircuits is largely conserved across areas, it might well be that MI is also layer and cell type specific in multisensory cortices.

The mouse is an ideal model organism to study the cellular substrates of MI, because subpopulations of neurons can be identified and studied using a combination of genetic, electrophysiological and optical methods. Multisensory responses in rodents are mostly found in transition stripes located between primary cortices (Wallace et al., 2004). Recent work identified several association areas around V1 (Wang and Burkhalter, 2007), differing in their response properties (Andermann et al., 2011; Marshel et al., 2011; Roth et al., 2012) as well as in connectivity (Wang et al., 2012).

Here, we investigated the cellular basis of MI in a bimodal (somatovisual) area located between V1 and S1. By combining intracellular recordings and functional two-photon imaging, we examined (1) whether MI is different for synaptic inputs (postsynaptic potentials—PSPs) and for action potential (AP) outputs, (2) how MI impacts unisensory processing, (3) whether MI is different in excitatory and inhibitory cells and which is the functional impact of these cell-type-specific differences for MI for the network output, and finally (4) whether there is a topographical organization of unimodal and bimodal cells, both across the cortical surface and across cortical layers. Our results provide one of the first mechanistic dissections of the synaptic, cellular and network organization of MI in the neocortex.

RESULTS

A Bimodal (Visuotactile) Area between V1 and S1

We targeted a visuotactile area between the rostral V1 and the caudal S1 (Wallace et al., 2004), corresponding to area RL (Figure 2 of Wang and Burkhalter, 2007), by using intrinsic optical imaging (IOI). To this purpose we stimulated the lower visual field (which activates rostral V1) and the most caudal whiskers (to stimulate the caudal-most part of S1—see Figures 1A and 1B and Experimental Procedures). Area RL could also be indentified cytoarchitectonically as the region with reduced cytochrome oxidase staining located between V1 and S1 (Figure 1C). IOI-targeted extracellular multiunit recordings

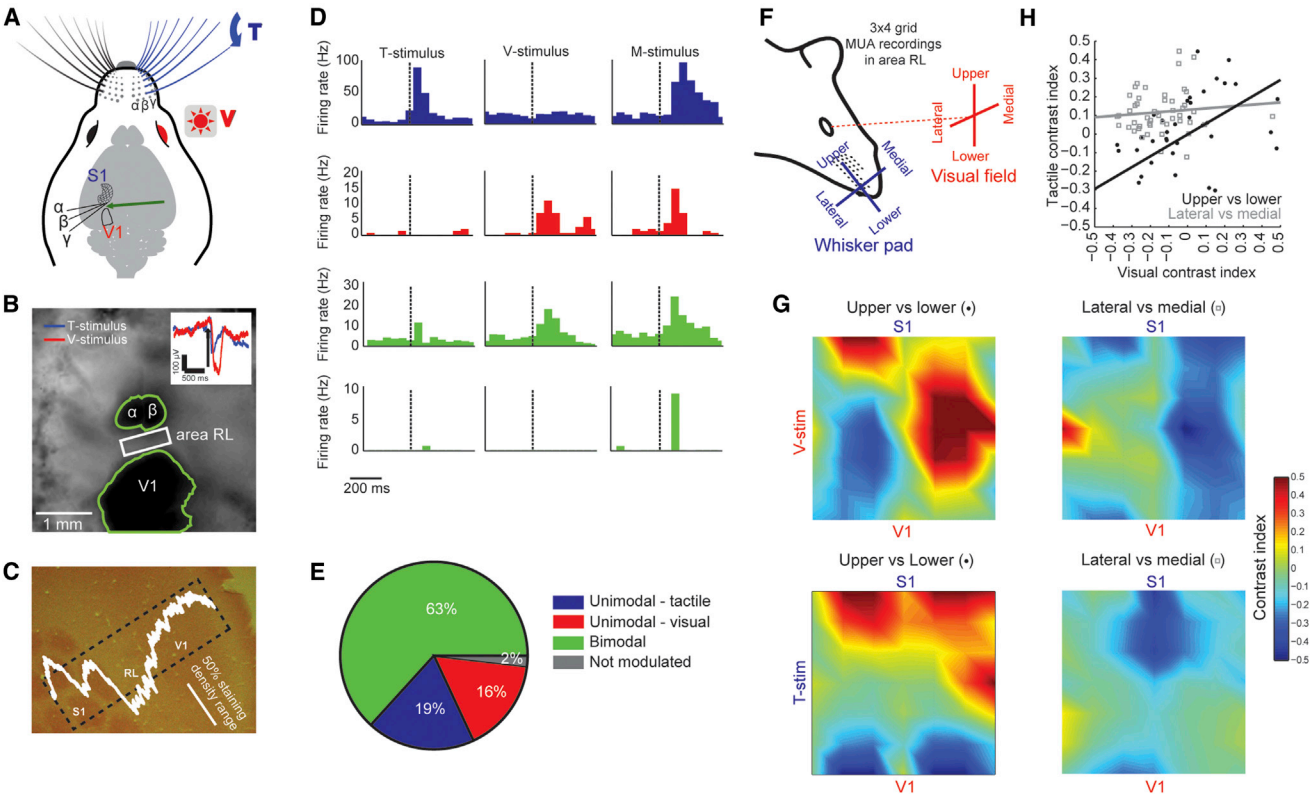

Figure 1. A Visuotactile Area between V1 and S1: Topographic Organization

(A) Mice were presented with a visual stimulus (flash, V) or a tactile stimulus (whisker pad deflection, T). Green arrow indicates RL, between rostral V1 and the caudal barrels (S1).

(B) IOI was used to target recording in area RL, as comprised by the α and β barrels and rostral V1. Green lines are area borders (see Experimental Procedures). White rectangle: RL. Inset: field potential in the middle of RL (blue: T stimulus, red: V stimulus). Dark spots are the activated areas during IOI.

(C) Cytochrome oxidase- stained flattened tangential section showing the drop in staining intensity along the rostrocaudal S1-V1 axis in correspondence of RL. Cytochrome oxidase (CO) staining was quantified as the optical density along the longer side of the rectangle (corresponding to the V1-S1 axis).

(D) AP responses to T, V, and M stimulations for a tactile unimodal cell (blue), a visual unimodal cell (red) and two bimodal cells (green). Dashed lines: stimulus onsets. Bin: 50 ms.

(E) Proportions of bimodal, tactile unimodal, visual unimodal and non responsive (gray) units, recorded below 300 μm.

(F) The topographic organization of sensory responses was evaluated by subdividing both the visual field (red) and the whisker pad (blue) into four corresponding half-planes: upper and lower, and medial and lateral fields. Sensory stimuli were presented while recording multiunit activity (MUA), with a 3 × 4 electrode grid in RL.

(G) Smoothed color maps showing the average values of half-plane dominance indexes across area RL for visual (top row) and tactile (bottom row) stimulations. The half-plane dominance index is shown for upper versus lower fields (left) and lateral versus medial fields (right).

(H) Relationship between visual (x axis) and tactile (y axis) half-plane dominance indexes for upper versus lower field stimulation (black dots) and lateral versus medial field stimulation (gray squares). A significant correlation between the two maps was found between tactile and visual half-plane dominance indexes for upper versus lower field stimulation ($r = 0.58$, $p < 0.05$), but not for lateral versus caudal field stimulation ($r = 0.11$, p-value = 0.44).

See also Figure S1.

indicated the coexistence of unimodal and bimodal neurons in RL (Figure 1D). We used a full-field flash as visual stimulus (V stimulus) and deflection of the whisker pad as tactile stimulus (T stimulus), and we defined units as bimodal or unimodal depending to whether they showed a significant response to one or both sensory modalities, independently presented (see Experimental Procedures). The majority of units (n = 171 from 9 mice) were bimodal (63%), whereas 35% were unimodal (16% driven by V stimulation and 19% by T stimulation—Figure 1E and see Figure S1A available online). Units that were not driven by tactile stimulation of the whiskers could be driven by somatosensory input from body parts different from the whiskers. To control for this, we stimulated the contralateral hind- and forelimbs and the trunk. However, we did not find detectable responses in RL (Figures S1B and S1C), indicating that the predominant or exclusive source of tactile input to RL is from the whiskers.

We next investigated whether there was a topographical organization of unisensory responses in RL, and, if so, whether the two sensory maps were aligned. We used 3 × 4 grids of extracellular electrodes covering all of RL (see Experimental Procedures). For unimodal sensory input, we separately stimulated the upper/lower and medial/lateral halves of both visual space and the whisker pad (Figure 1F). For each neuron, we

computed a relative preference index as (U − L)/(U + L), where U and L are the neuronal responses to the upper or lower visual or tactile field stimulations, respectively. Then we averaged the relative spatial preference indexes of all neurons along a given position of the grid. We finally mapped the spatial preference within RL for the upper versus lower and medial versus lateral stimulation for both modalities (Figure 1G). In line with (Marshel et al., 2011; Wang and Burkhalter, 2007) we found a retinotopic map within RL, but we also found a spatial segregation between responses elicited by the upper or lower aspects of the whisker pad. For example, the rostral part of RL preferentially responded to the upper visual field and to the upper whiskers. To quantify the degree of alignment between the two maps, we computed the correlation between the retinotopic and tactile maps along the same spatial direction (upper-lower and medial-lateral axes separately; Figure 1H). We found a significant degree of spatial alignment of the somatic and visual spatial preference maps along the upper-lower axis of the sensory space (black circles; $r = 0.58$, $p < 0.001$) but a weaker and nonsignificant alignment along its mediolateral axis (gray squares; $r = 0.11$, $p = 0.44$).

Synaptic Potentials Were More Bimodal Compared to Spike Responses but Showed Less Multisensory Enhancement

We next compared bimodality and MI at the level of PSPs and of APs by IOI-targeted whole-cell recordings from layer 2/3 pyramids (n = 46 from 12 mice; Figure 2A).

First, bimodal neurons were more abundant for PSPs (56% of responsive cells) compared to APs (39% of them; Figure 2B). Indeed, many neurons that were bimodal for PSPs were unimodal for APs (see example of Figure 2C): out of 24 neurons that were bimodal for PSPs, only 11 (46%) were bimodal for APs, 4 (17%) were unimodal and 9 did not respond with APs. Also, some cells with bimodal PSPs responded with APs only when V and T stimuli were simultaneously presented (multisensory—M stimulation; see example of Figure 2D).

Second, we compared MI for PSPs and APs. Multisensory neurons display a response to a cross-modal combination of stimuli that is enhanced compared to the preferred unisensory stimulus (Stein and Stanford, 2008). To quantify such multisensory enhancement (ME), we computed an ME index, defined as $(M - \max(V,T))/\max(V,T)$, where M is the response to M stimulation, and max(V,T) is the highest unimodal response. To measure M responses, we set the delay between V and T stimuli equal to the delay between V and T responses so to maximize the interaction (137.1 ± 15.2 ms). Synaptic responses to M stimulation were larger than responses to the preferred unimodal stimulus (Figure 2E; 11.9 ± 1.0 mV versus 9.3 ± 0.8 mV, paired t test, $p < 0.0001$). ME was even larger for APs (Figure 2F; medians: 4.6 versus 3.0 Hz; paired Wilcoxon rank-sum test, $p < 0.05$). A paired comparison between the ME indexes for PSPs and APs for each cell indicated that ME was consistently larger for APs (Figure 2G; top; medians: 0.80 versus 0.29; Wilcoxon rank-sum test, $p < 0.01$).

Response summation was sublinear for PSPs, i.e., M responses were smaller than the sum of unimodal responses. However, this was not the case for AP responses. To examine this quantitatively, we calculated for each neuron a linearity index defined as $(M - (V+T))/(V+T)$, where V, T, and M are the amplitude of the responses to V, T, and M stimulation, respectively. This index is negative for a sub-additive integration and positive for supra-additive integration. This index was in most of the cases negative for PSPs and either null or positive for APs (Figure 2G, bottom; medians: −0.18 for PSPs and 0.06 for APs, $p = 0.02$, Wilcoxon rank-sum test).

In summary, MI was qualitatively and quantitatively different for synaptic inputs and spike outputs: more neurons were bimodal for PSPs than APs, ME was larger for APs, and MI was subadditive for PSPs but additive (or supra-additive) for APs.

Multisensory Integration Was Scarcer in Layer 5

We next performed IOI-targeted whole-cell recordings from pyramids in the deep cortical layer 5 (the main output layer of the cortex; n = 25 from 6 mice) to compare MI in layer 5 and in layer 2/3 pyramids.

First, the proportion of bimodal neurons was higher in layer 5 than in layer 2/3, for both PSPs and APs (Figure 3A; PSPs: 92% versus 56%; APs: 68% versus 39%). However, ME was scarcer among layer 5 pyramids: bimodal neurons had smaller differences between unisensory and multisensory responses compared to layer 2/3 (compare Figure 3B to Figures 2C and 2D). For layer 5 pyramids, PSP responses to M stimuli were indistinguishable from responses to the preferred unisensory stimulus (Figure 3C; 8.2 ± 0.7 versus 8.0 ± 0.9 mV; paired t test, $p = 0.68$). The same was true for AP responses (Figure 3D; medians: 5.0 versus 5.1 Hz; paired Wilcoxon rank-sum test, $p = 0.88$). The ME indexes for both PSP and AP responses of layer 5 pyramids were significantly lower compared to layer 2/3 pyramids (Figure 3E; medians for PSPs: 0.02 versus 0.29; for APs: −0.03 versus 0.6; Wilcoxon rank sum tests, $p < 0.01$ for both comparisons). Similar results were found for extracellular multiunit activity (see Supplemental Text, Figure S3, and Table S1).

In summary, although we found more bimodal neurons in infragranular layers, those neurons displayed less ME compared to supragranular neurons, and this was already evident for synaptic inputs in layer 5.

Tactile Stimuli Preferentially Enhanced Nonoptimal Visual Responses

We next investigated whether bimodality in area RL might aid sensory processing of weak unisensory stimuli. To simultaneously analyze as many cells as possible, we performed two-photon population calcium imaging after bolus loading of the calcium indicator Oregon green BAPTA-1 in the center of area RL (Figure 4A). Figure 4B shows an example of the spatial distribution of unimodal and bimodal cells, as defined by their calcium responses (see Experimental Procedures) within an optical plane. Examples of single trial and averaged calcium fluorescence changes in response to unimodal and bimodal stimulations are shown in Figure 4C.

To address our question, we exploited the fact that many RL neurons are directionally selective to moving visual stimuli (Marshel et al., 2011). We used squared gratings drifting in either the rostro-to-caudal or caudo-to-rostral direction (Figure 4D and see Experimental Procedures). We found that many

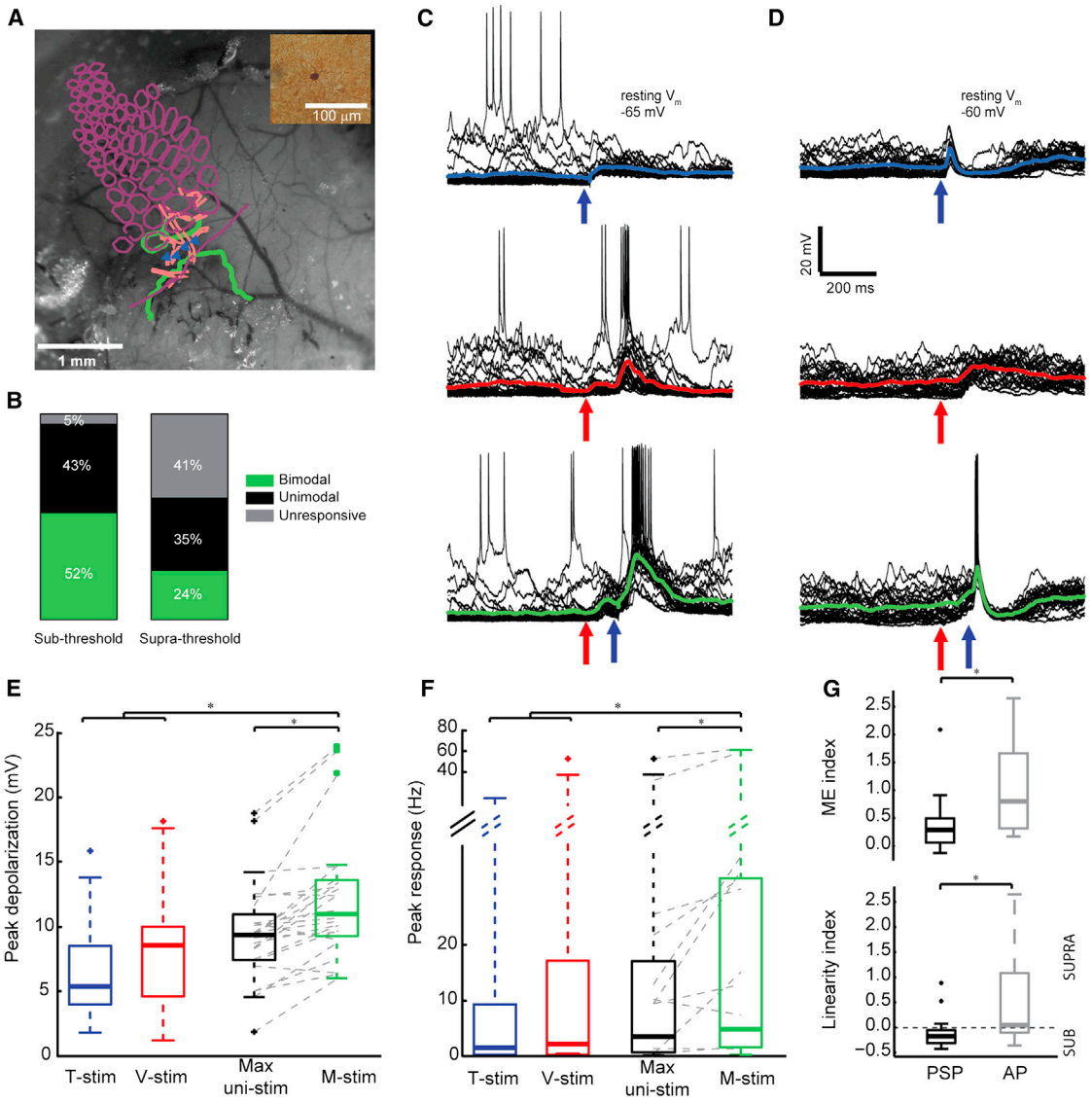

Figure 2. Synaptic Potentials Were More Bimodal Compared to Spike Responses, but Showed Less Multisensory Enhancement

(A) Patched, biocytin-filled layer 2/3 pyramids in RL. CO-stained flattened tangential cortical sections were registered by aligning blood vessels visible on the fixed slice surface (pink) with the blood vessel image taken through the skull before IOI. V1 and barrels borders, detected by IOI (green) or by CO staining in the fixed slide (purple) coincided and allowed unambiguous identification of RL. Blue marks: positions of biocytin-filled pyramids in the slice (inset).

(B) Proportion of unimodal (black) and bimodal (green) cells at PSP and AP level (left and right) in layer 2/3. Gray: unresponsive cells.

(C) A neuron that was bimodal at PSP level, but appeared unimodal at AP level. The consequence was an enhanced AP response upon M stimulation (bottom). Single trials are overlaid and the average PSP is the colored, thicker line. Arrows: onsets for V and T stimuli.

(D) This neuron produced APs only upon M stimulation, but displayed PSPs to both unimodal stimuli.

(E) PSP responses of layer 2/3 pyramids to T (blue), V (red), and M (green) stimuli and to the preferred unimodal stimulus (black). PSPs to M stimuli were significantly larger than both unimodal responses, and also than the response to the preferred unimodal stimulus ($p < 0.05$ for both comparisons).

(F) Same as in (E) for AP responses.

(G) Top: The ME index for APs (gray) was larger compared to PSPs (black) ($p < 0.01$). Bottom: Linearity indexes of PSPs were smaller than 0 (black, $p < 0.01$), indicating a sublinear integration for PSPs, and were also smaller compared to APs ($p < 0.05$).

See also Figure S2.

RL neurons were selective for the direction of the stimulus: their direction-selectivity index, defined as (Pref − NonPref)/(Pref + NonPref)—where Pref and NonPref are the responses to the preferred and non preferred direction, respectively, was on average 0.79 ± 0.33 (119 responsive cells from 7 mice), in line with a previous report (Marshel et al., 2011). The very same tactile stimulus (an air puff to the whisker pad directed rostrocaudally) was then presented simultaneously with either the preferred or the nonpreferred visual stimulus. On average, the tactile stimulus increased the response to the

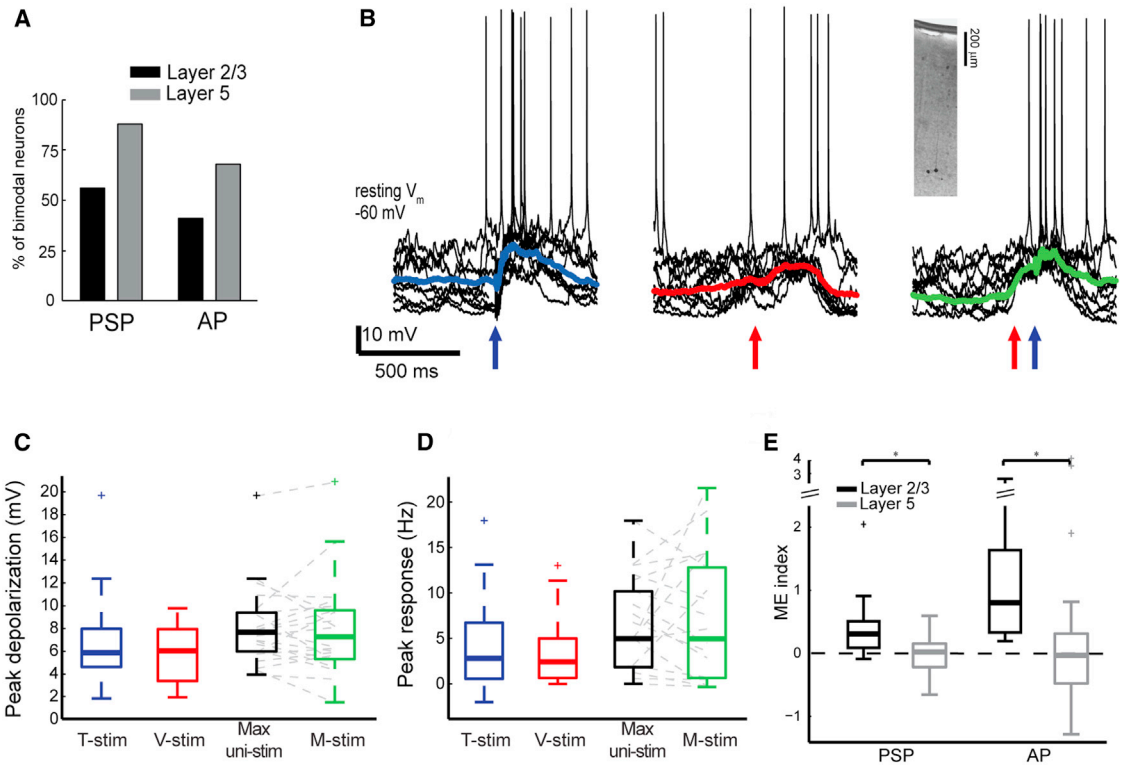

Figure 3. Scarce Multisensory Enhancement in Layer 5 for Both Synaptic and Spike Responses

(A) Bimodal cells (as % of responsive cells) were more abundant in layer 5 than in layer 2/3 (gray and black), for both PSPs and APs.

(B) A whole-cell recording from a layer 5 pyramid (inset), showing its response to T (left), V (center), and M (right) stimuli. Single trials are overlaid and the average PSP is the colored line. Arrows indicate stimulus onsets. Note the scarce response enhancement upon M stimulation.

(C) PSP responses of layer 5 pyramids to T (blue), V (red), and M (green) stimuli, and to the preferred unimodal stimulus(black). PSPs to M stimuli were statistically indistinguishable from PSPs evoked by the preferred unimodal stimulus ($p > 0.05$).

(D) Same plots as in (C) for AP responses of layer 5 pyramids.

(E) The ME indexes of layer 2/3 pyramids (black) were larger compared to layer 5 pyramids (gray) for both PSPs and APs ($p < 0.05$).

See also Figure S3.

nonpreferred visual direction significantly more than the preferred visual direction (Figure 4F; 119 neurons; average enhancement 52% versus 0%, paired Wilcoxon rank-sum test, $p < 0.001$).

Hence, a given unimodal stimulus selectively enhances responses to the nonpreferred stimulus configuration of the other modality, in line with the so called ''inverse effectiveness principle'' described in other multisensory areas in the mammalian brain (Stein and Stanford, 2008).

Spatial Density Gradients of Unimodal Neurons Oriented toward the Corresponding Primary Cortex

We next investigated the spatial distribution of unimodal and bimodal cells by means of population calcium imaging. Figure 5A shows the overlay of all imaged, responsive neurons (34%, 503/1480 labeled neurons from 10 mice), where each cell is positioned along the rostrocaudal (S1-V1) axis with respect to the midline of RL. The mean positions of unimodal neurons were statistically different, with tactile cells (T cells) closer to S1 and visual cells (V cells) closer to V1 (Figure 5B; mean distances from midline: -4.8 ± 5.2 µm for T cells, 23.4 ± 5.5 µm for V cells and 4.6 ± 5.9 µm for multimodal cells (M cells), $p < 0.01$, one-way ANOVA, $n = 165$, 176, and 162, respectively; Tukey post-hoc: $p < 0.01$ for T and V cells, $p = 0.08$ for V and M cells, $p = 0.53$ for T and M cells). To investigate whether the positions of unimodal neurons follow a gradient along the V1-S1 axis, we divided the imaged area in three stripes orthogonal to the rostrocaudal axis. Because cell loading with OGB-1 was more pronounced near the center of the field of view (where the dye injections were targeted; Figure S4A), we normalized the numbers of responsive cells for the total number of labeled cells in each stripe. The percentage of unimodal cells decreased with the distance from the border of the respective primary area (solid lines in Figure 5C, left). Conversely, bimodal cells were uniformly distributed, with a slight increase in the middle of the field of view. To test for a gradient in the density of unimodal cells along the V1-S1 axis, we performed a linear regression on the cell-density values (dashed lines in Figure 5C, left) For unimodal cells, the slopes were significantly different from zero (see Figure 5C, right; slopes: -0.066 for T cells, $p = 0.017$; 0.078 for V cells, $p = 0.005$; permutation test for the slope; see Supplemental Experimental Procedures). The distribution of bimodal cells did

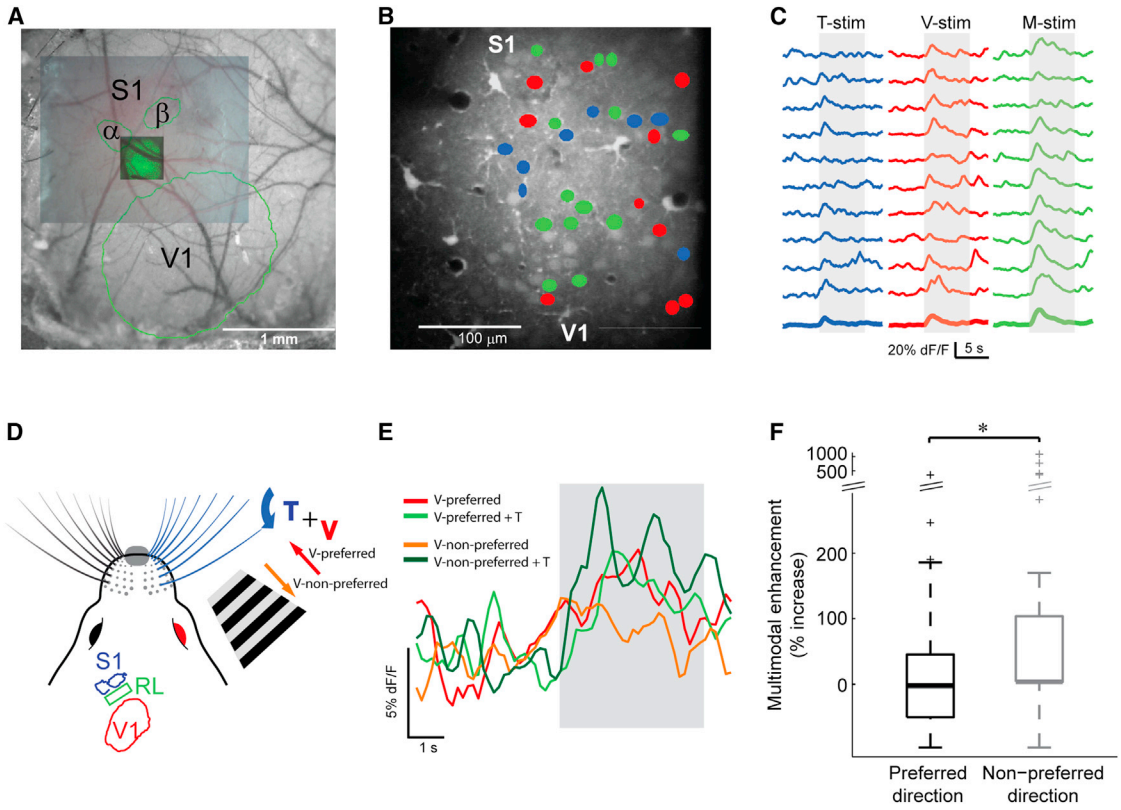

Figure 4. Population Calcium Imaging Revealed Inverse Effectiveness in RL

(A) IOI-targeted bolus loading of OGB-1. V1 and S1 borders (green) are outlined on the vasculature (larger) image taken under the IOI system. The medium-sized vasculature image was taken with a 4× objective in the two-photon setup and was aligned to the first. After two-photon imaging, the location of the loaded region (green spot of OGB-1 fluorescence) was verified by aligning blood vessels shown by a z projection of the loaded tissue (smaller inset) with the vasculature image taken with the 4× objective.

(B) Spatial distribution of bimodal (green) and unimodal cells (red: V driven; blue: T driven) in one optical plane (40× objective) in layer 3.

(C) Example of calcium fluorescence responses of a bimodal neuron, showing single traces (thin) and average responses (thick). The stimulus (T, blue; V, red; M, green) was presented for 8 s (shadowed areas) after 8 s of baseline.

(D) To investigate the presence of inverse effectiveness in RL, calcium imaging was performed while a drifting grating was shown in the preferred (red arrow) or non-preferred (orange arrow) direction. The whisker pad was stimulated with an air puff (blue arrow), simultaneously with either the preferred or nonpreferred grating.

(E) This RL neuron showed a differential response for the two direction of visual stimulation (red: preferred; orange: nonpreferred). When the T stimulus was superimposed to the V stimulus, the response to the V-nonpreferred stimulus (dark green) was enhanced more than that to the V-preferred stimulus (light green).

(F) RL neurons display inverse effectiveness. The same tactile input enhanced more responses to the nonpreferred direction (gray) than those to the preferred direction (black, $p < 0.001$).

not show a spatial gradient (−0.012 for M-driven cells, $p = 0.68$; permutation test for the slope). Moreover, we failed to find a similar gradient for a modality dominance index—which expresses the relative strengths of the two modalities—computed on responses of bimodal cells (Figure S4B). This indicated that bimodal cells near one primary cortex were not functionally dominated by the corresponding modality.

Microclusters of Unimodal Neurons in the Center of RL

We then wondered whether the three types of responsive neurons showed some kind of spatial clustering on a microscale level. Since the gradient of unimodal neurons could be a confounding factor, we restricted our analysis to the middle stripe of the imaged area (i.e., a portion of RL oriented orthogonal to the V1-S1 axis and equidistant from both S1 and V1—see also additional controls in Table S2). Within this stripe the mean position and density of cell somata along the V1-S1 axis were statistically indistinguishable for V, T, and M cells, indicating a homogenous distribution of unimodal neurons within the central cortical stripe (Figures S4C and S4D). We performed a nearest-neighbor analysis in the center of area RL for V, T, and M cells separately on single optical planes (Komiyama et al., 2010; Figure 5D). As the three cell types had a similar density, we took 0.33 as a chance probability for the nearest neighbor analysis (Figure 5E).

For each cell type, we first computed the probability of having a nearest neighbor of a certain type. For unimodal cells, the probability that the nearest neighbor was another unimodal neuron of the same modality was above chance (Figure 5E; for T cells: 52.5% of T neighbors, $p < 0.001$; for V cells: 55.7% of V

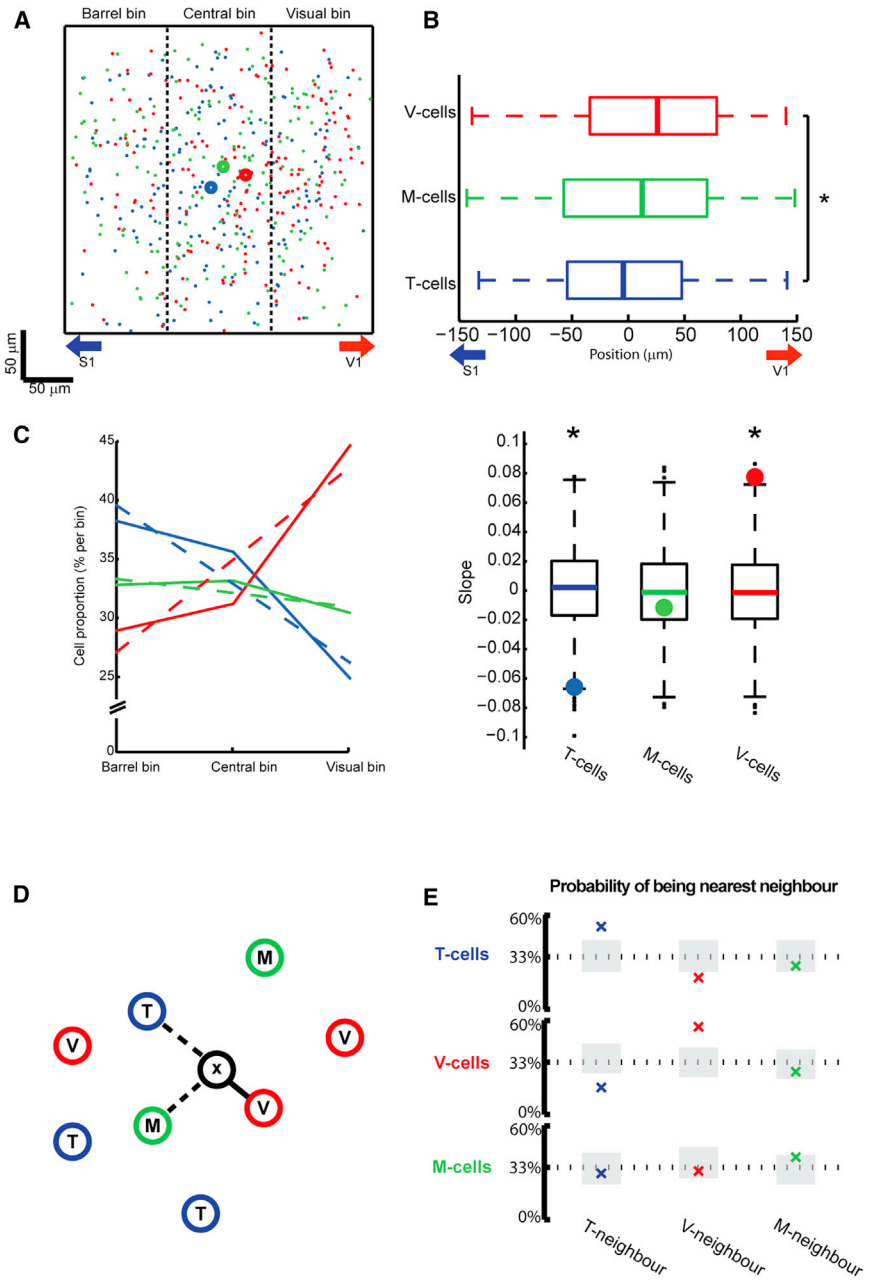

Figure 5. Microarchitecture of Unimodal and Bimodal Neuron Distribution in Area RL

(A) Overlay of the fields of view showing the positions of all responsive neurons relative to the injection site—corresponding to the midline (blue: T cells, red: V cells, green: bimodal cells). The dashed lines indicate the subdivision into three spatial bins: near-S1 bin, central bin, and near-V1 bin.

(B) Positions of the somatas of T-driven, V-driven, and M-driven neurons along the rostrocaudal, V1-S1 axis. T-driven cells were closer to the S1 border compared to V-driven cells ($p < 0.01$).

(C) Left: Relative proportion of T (blue lines), V (red lines), and M (green lines) cells in the barrel, central and visual bins. Actual values (solid lines) and fitted trends (linear regression, dashed) are shown. Right: Boxplots showing slope values obtained by randomly permuting cell labels and recomputing the fits (see Supplemental Experimental Procedures). Circles indicate actual values. The actual slope was significantly different from that of the random distribution for both T ($p < 0.05$) and V neurons ($p < 0.01$), but not for M cells, indicating the existence of a significant gradient in the density of unimodal cells along the V1-S1 axis.

(D) Nearest neighbor index computation. For each cell (cell X, black circle) the distances to the closest T-driven (blue circles), V-driven (red circles), and M-driven (green circles) cells were found (both dashed and solid lines). The closest of these three cells was identified as the nearest neighbor (solid line).

(E) For each cell type, the probability of having as nearest-neighbor a T-driven (blue cross), a V-driven (red cross), or an M-driven (green cross) neuron is shown. Gray areas show the confidence intervals for the null hypothesis, i.e., that all three cell types have the same probability of being the nearest neighbor of a given neuron. Both classes of unimodal neurons had a higher than chance probability to be closer to another unimodal neuron driven by the same modality, but a lower than chance probability to be closer to another unimodal cell driven by the other modality, while no significant deviation from chance was observed for M-driven, bimodal cells.

See also Figure S4 and Table S2.

neighbors, $p < 0.001$) and the probability that the nearest neighbor was a unimodal neuron but driven by the other modality was below chance (for T cells: 17.1% of V neighbors, $p < 0.01$; for V cells: 20.0% of T neighbors, $p < 0.05$). For unimodal cells, the probability that the nearest neighbor was bimodal did not differ from chance. Conversely, for bimodal cells, the nearest neighbor could either be a T, V, or M cell, with a trend toward M cells (29.4% of T neighbors, $p = 0.58$, 30.9% of V cells, $p = 0.27$, 39.7% of M neighbors, $p = 0.12$, bootstrap test—see Experimental Procedures). As a second measure of spatial clustering, we computed, for each cell type, the distance of the closest T, V, or M cell (Figure S4E and Supplemental Text). This analysis confirmed that unimodal neurons were closer to other unimodal neurons of the same modality, compared to the other cell types, whereas no significant trend for clustering was found for bimodal cells.

Scarcer Multisensory Enhancement in Parvalbumin-Positive Interneurons Compared to Pyramids

We next examined MI in the major class of inhibitory interneurons (parvalbumin-positive interneurons—Pv-INs), using two-photon-targeted juxtasomal recordings. We used mice expressing the red fluorescent protein tdTomato selectively in Pv-INs (*tdTomato flox/flox;Pv Cre* mice; Figure 6A). For comparison, we also recorded from pyramids, by "shadow patching" to identify the pyramidal somatas (Figure 6C). Pv-INs displayed high-frequency

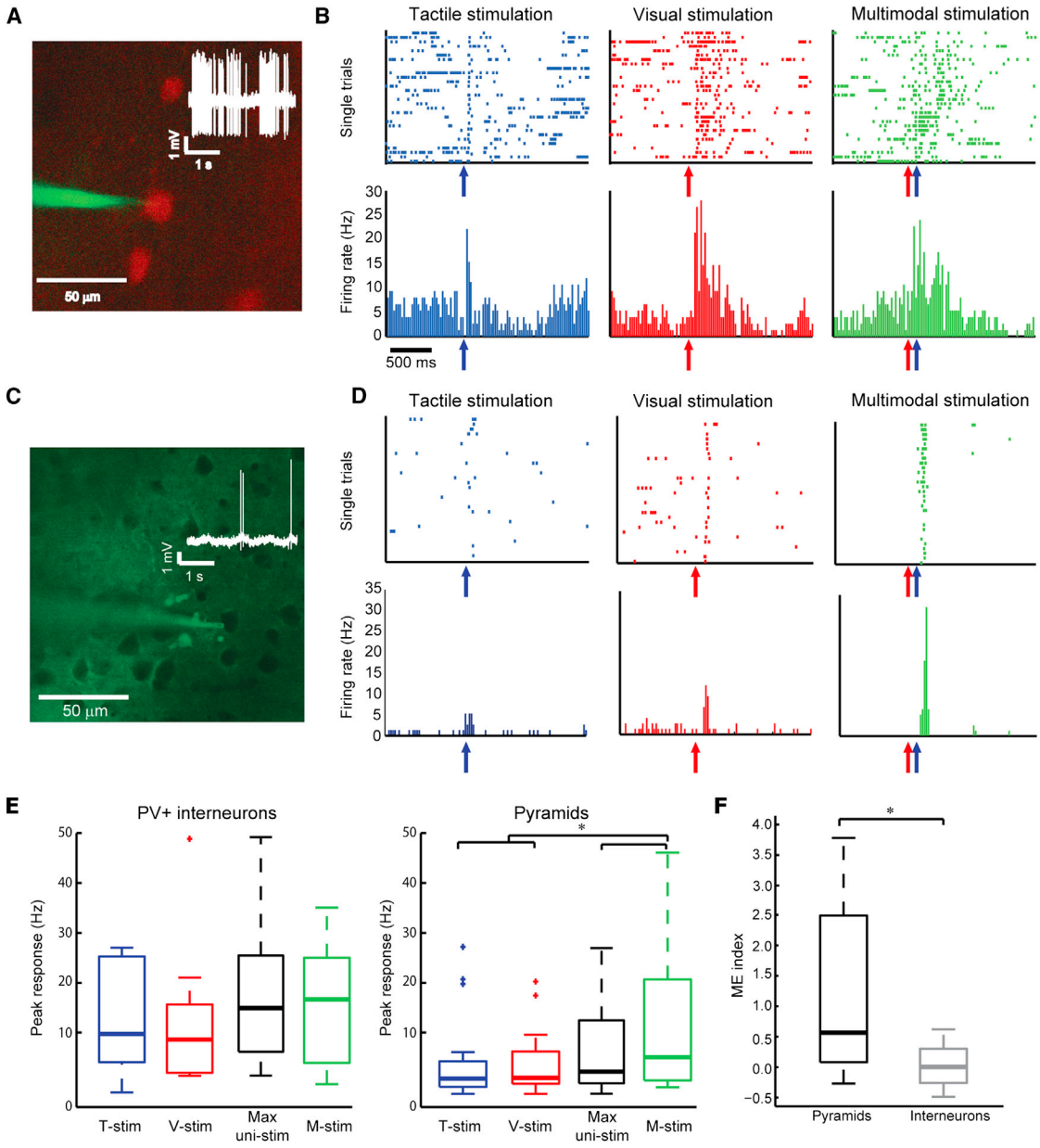

Figure 6. Parvalbumin-Positive Interneurons Have Much Scarcer Multisensory Enhancement Than Pyramids

(A and B) Example raster plots (top) and peristimulus time histograms (bottom) for a two-photon-targeted juxtasomal recording of a bimodal Pv-IN upon T, V, and M stimulation (blue, red, middle and green, respectively) from a mouse expressing the red protein tdTomato selectively in Pv-INs (the pipette is filled with the green Na^+-salt dye Alexa 488). Note the high-frequency bursts of APs with deep afterhyperpolarizations (white). Arrows are stimulus onsets.

(C and D) Same as in (A and B) but for a regular-spiking pyramid targeted under the two-photon with the "shadow patching" technique (Alexa 488 being gently ejected in the extracellular matrix to visualize pyramidal cell bodies as dark structures. Note the more pronounced ME in the regular-spiking pyramid compared to the Pv-IN.

(E) Boxplots showing responses of Pv-INs (left) and regular-spiking pyramids (right) to T (blue), V (red), and M (green) stimuli and to the preferred unimodal stimulus (black), all recorded in juxtasomal configuration. The M response was statistically similar to the preferred unisensory responses for Pv-INs ($p = 0.9$), but it was larger in pyramids ($p < 0.05$).

(E) ME indexes of pyramids were larger compared to Pv-INs ($p < 0.05$).

firing of narrow APs (Figure 6A, inset; n = 20 from 6 mice, AP half-width 382 ± 41 µs), whereas pyramids had regular-spiking firing patterns with broader APs (Figure 6C, inset; n = 28 from 5 mice, AP half-width 498 ± 29 µs).

Pv-INs were more often bimodal compared to pyramids (66%—12/18 responsive cells versus 39%—11/28 cells, respectively). Figures 6B and 6D compare the AP responses of a Pv-IN and a pyramid in response to unisensory and multisensory

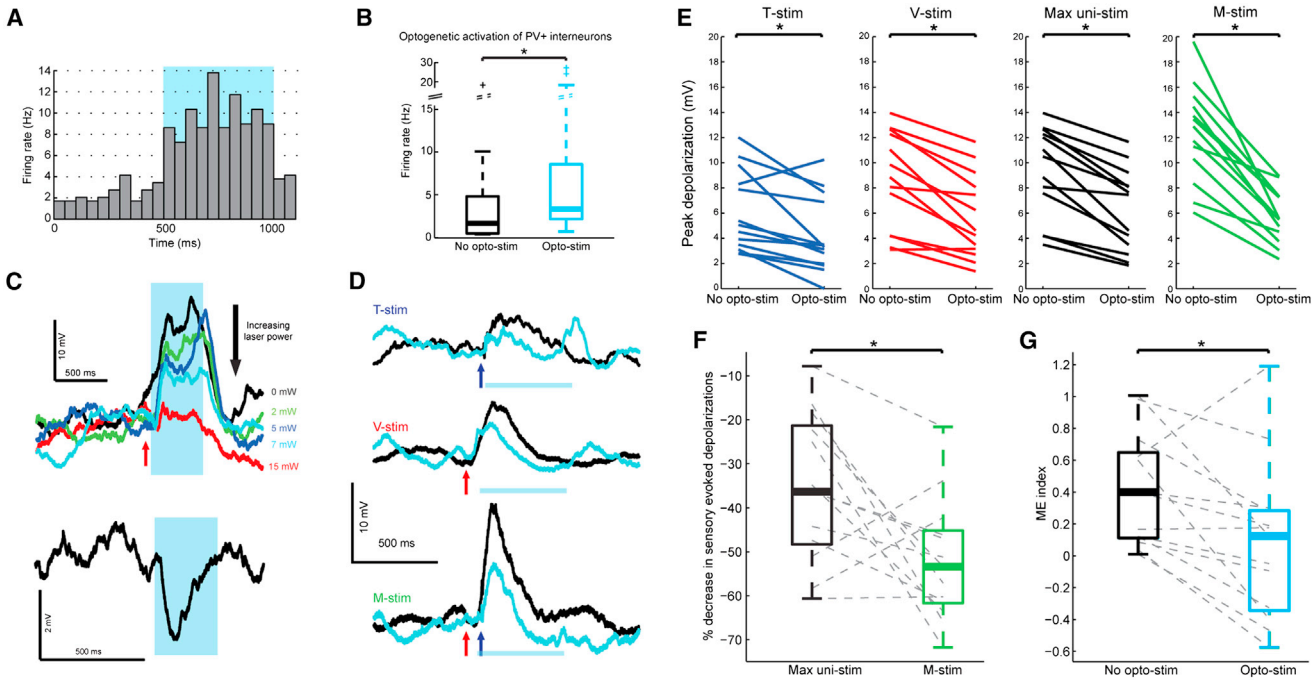

Figure 7. Optogenetic Activation of Parvalbumin-Positive Interneurons Selectively Impairs Multisensory Enhancement of Synaptic Inputs in Neighboring Pyramids

(A) Increase in firing rate of an extracellularly-identified Pv-IN following blue laser light stimulation (shaded).

(B) Boxplots showing overall increase in AP rates of extracellularly identified Pv-INs during photoactivation (blue) compared to baseline (black).

(C) Top: Modulation of the laser power (blue area) can progressively inhibit sensory-driven (here visually driven) PSPs in pyramids (red arrow: stimulus onset). For all experiments, laser power was set so to reduce PSPs to unisensory stimuli of about 1/3 (here 7 mW). Bottom: In the absence of sensory stimuli, Pv-IN photostimulation at that intensity elicited an IPSP in the pyramidal cell.

(D) Example of synaptic responses of a single pyramidal cell following T (top), V (middle), and M (bottom) stimuli in the absence (black) and presence (blue) of Pv-IN photoactivation. Arrows are stimulus onsets, whereas blue lines indicate laser photostimulation. Pv-IN photoactivation reduces M responses relatively more than unisensory responses.

(E) Sensory-evoked PSPs with and without photoactivation of Pv-INs ("Opto-stim"). Both unisensory (red: visual, blue: tactile, black: preferred unisensory) and M responses were reduced by Pv-IN photostimulation, but the effect was proportionately larger for M responses.

(F) The relative (%) decrease of sensory-evoked PSPs due to Pv-IN photostimulation was larger for M responses (green) compared to responses to the preferred unisensory stimulation (black; $p < 0.05$).

(G) ME indexes for synaptic responses measured from pyramids dropped significantly upon Pv-IN photostimulation (blue versus black; $p < 0.05$).

See also Figure S5.

stimulations. In general, we found that ME was less pronounced in Pv-INs. Indeed, M responses of Pv-INs were not different from the preferred unimodal responses (Figure 6E, left; medians: 16.24 versus 15.04 Hz, respectively; Wilcoxon rank-sum test, $p = 0.91$). In contrast, M responses of pyramids were larger than their preferred unimodal responses (Figure 6E, right; medians: 3.95 versus 6.52 Hz, Wilcoxon rank-sum test, $p < 0.05$). Thus, ME indexes were on average larger for pyramids (Figure 6F; medians: 0.57 versus 0.01, respectively; Wilcoxon rank-sum test, $p < 0.05$).

The general lack of ME among Pv-INs could be due to a mix of cells with either enhancement or suppression upon M stimulation. However, a single-trial analysis for individual cells showed that, out of the 12 bimodal Pv-INs, only four showed enhanced responses to multimodal stimulation; two showed reduced responses and six showed no difference. Thus; ME was more consistent in pyramids than in Pv-INs of layer 2/3.

Optogenetic Activation of Pv-INs Selectively Impairs Multisensory Enhancement in Pyramids

We then investigated whether the scarce ME in Pv-INs could enable a more robust ME in neighboring pyramids. Indeed, pyramids show strong ME during multisensory stimulation, but Pv-INs show very little increase in firing for multisensory versus unimodal stimulation. This suggests that pyramids could receive more excitatory input—with proportionately less inhibition—during M stimulation than during unisensory stimulation. To examine this potential mechanism, we tested whether selectively increasing the firing of the Pv-INs during M stimulation selectively impacts ME in pyramids, possibly by promoting MI in at least a portion of Pv-INs.

We selectively activated Pv-INs using optogenetics. We obtained mice expressing the channelrhodopsin channel only in Pv-INs by crossing mice expressing Cre-recombinase under the Pv promoter with mice bearing a floxed-Channelrhodopsin construct (Madisen et al., 2012). We thus had an optogenetic

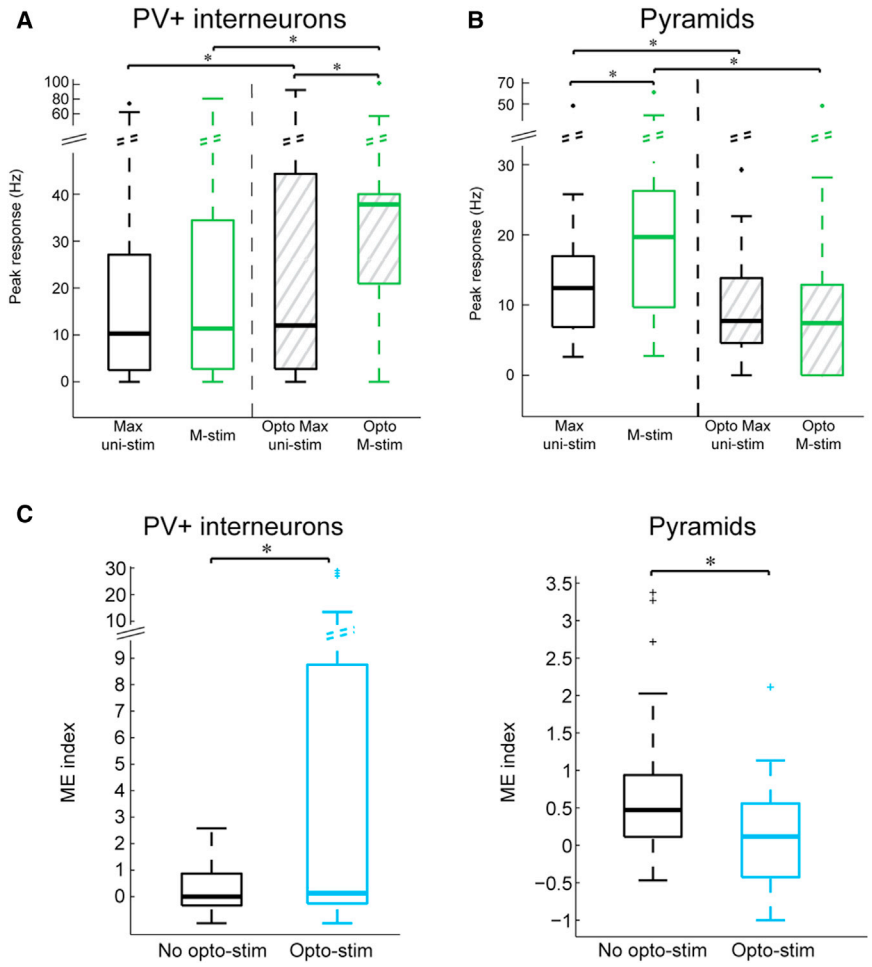

Figure 8. Photoactivation of Parvalbumin Interneurons Promotes Multisensory Enhancement of Their Spike Output

(A) AP responses of Pv-INs following M (green) stimuli and the preferred unimodal stimulus (black), without and with photostimulation (open and dashed boxes, respectively). M responses were larger than those to the preferred unisensory stimulus only during laser activation (*$p < 0.05$), i.e., photoactivation of Pv-INs selectively promoted MI in the population AP output of this interneuronal subpopulation.

(B) Same plot as in (A) for putative pyramidal cells. Responses to M stimuli were statistically indistinguishable from those to the preferred unisensory stimulus during laser activation only ($p < 0.05$). Thus, ME of pyramids was selectively inhibited by Pv-IN photoactivation.

(C) Opposite effects of Pv-IN photoactivation on ME indexes of Pv-INs and pyramids. Pv-IN photostimulation increased the ME index of their AP responses (left), while it reduced the ME index of putative pyramids (right; $p < 0.05$).

See also Figures S5 and S6 and Tables S3 and S4.

tag to identify Pv-INs by combining extracellular recordings and blue laser activation. We confirmed that laser stimulation selectively activated Pv-INs by verifying three criteria: (1) laser photostimulation activated a cell at short latencies (Figures 7A and 7B); (2) the cell exerted inhibitory influences on other simultaneously recorded cells, as shown by spike cross-correlograms (see Supplemental Experimental Procedures; Figure S5B); (3) they had on average higher AP rates than putative pyramids (see Figure S5A). Next, we performed whole-cell recordings in layer 2/3 pyramids to verify that Pv-IN photostimulation was able to reduce sensory-driven synaptic responses in a graded manner by varying laser power (Figure 7C, top). We set the power so to reduce the unisensory PSPs by approximately one-third (−34.8% ± 4.8%), and, when presented alone, Pv-IN photostimulation reliably induced IPSPs in pyramids (Figure 7C, bottom). This same photostimulation level significantly increased AP rates of Pv-INs within physiological values (Figure 7B; n = 34 cells from 5 mice; medians: from 1.4 Hz to 3.3 Hz, Wilcoxon rank-sum test, $p < 0.001$; see also Atallah et al., 2012).

We next compared the relative effect of Pv-IN stimulation on unisensory and multisensory synaptic responses of pyramidal cells. Figure 7D shows unisensory and multisensory PSPs without (black) and with (blue) laser activation during unisensory and multisensory stimulation. Pv-IN photostimulation consistently affected M responses more than either T or V unimodal responses (Figure 7E; n = 13 from 7 mice: T responses: 6.1 ± 0.9 mV versus 4.2 ± 0.8 mV, $p < 0.01$; V responses: 8.6 ± 1.1 mV versus 5.8 ± 0.9 mV, $p < 0.01$; preferred unisensory responses: 9.3 ± 1.0 mV versus 6.4 ± 0.9 mV, $p < 0.001$; M responses: 12.2 ± 1.0 mV versus 5.8 ± 0.6 mV, $p < 0.001$, paired t tests). Importantly, the relative (percent) decrease in PSPs was significantly smaller for unisensory responses than for multisensory responses (Figure 7F; −35.3% ± 4.3% versus −51.9% ± 3.8%; paired t test, $p < 0.05$). As a consequence, ME of pyramidal cells was dramatically but selectively reduced by Pv-IN photostimulation (Figure 7G; median ME indexes: 0.4 versus 0.1 without and with laser activation, respectively; paired Wilcoxon rank-sum test, $p < 0.05$).

To better understand a possible mechanism by which optogenetic activation of Pv-INs selectively disrupts ME in pyramids, we compared the activity of Pv-INs and putative pyramids during sensory stimulation with and without simultaneous laser activation. We therefore performed extracellular multi-unit activity recordings on putative Pv-INs and pyramids, identified following the three criteria described above. We first confirmed that for Pv-INs, M responses were comparable with their preferred unisensory responses in absence of photostimulation (Figure 8A; medians: 11.4 versus 10.3 Hz, Wilcoxon rank-sum test, $p = 0.35$). Conversely, M responses in Pv-INs became larger than the preferred unisensory responses upon photostimulation (37.8 versus 12.0 Hz, Wilcoxon rank-sum test, $p < 0.05$). Accordingly, the ME index for Pv-INs was increased by laser activation (Figure 8C, left; medians: 0.01 versus 0.13,

$p < 0.05$, paired Wilcoxon rank-sum test). The distribution of the ME indexes of Pv-INs upon photostimulation suggested that photostimulation increased the percentage of Pv-INs that displayed ME by ~50% with respect to no-photostimulation control condition (see single trial analysis for single cells of Tables S3 and S4). The analysis of the AP response of putative pyramids confirmed that Pv-INs photostimulation selectively disrupts ME in these cells (Figures 8B, 8C, and S6; Table S4). Note the opposite changes of the ME indexes for pyramids and Pv-INs upon photostimulation (decrease and increase, respectively).

The fact that optogenetically promoting integration in Pv-INs selectively disrupts ME in pyramids indicates that the lack of integration in Pv-INs enables the positive ME we observed in RL pyramidal neurons.

Functional Afferent Connectivity Underlying Multisensory Responses

To identify anatomical sources of multimodal inputs to RL, we performed IOI-targeted, retrograde tracers injections in RL (Figures 9A and 9B; see Experimental Procedures). Retrogradely labeled cells were found in V1 and S1 (Figures 9C and 9D) and, at subcortical level, in the associative PO thalamic nucleus (Figure 9E), but not in visual thalamus (dLGN and lateral posterior nuclei).

To characterize the role of corticocortical connections in shaping RL sensory responses, we had to overcome the problem that pharmacological blockade of the entire V1 or S1 would have invariably caused diffusion of the silencing agent into RL. We therefore exploited the retinotopic organization of the V1-to-RL projections. We performed IOI-targeted injections of the GABA-A agonist muscimol in caudal V1, which represents the upper visual field and projects to rostral RL (Wang and Burkhalter, 2007). We then recorded responses to upper and lower visual field stimulation in rostral RL, that preferentially responds to the upper field (Figure 9F), before and after fluorescent muscimol injection. The selective pharmacological blockade of caudal V1 was verified by IOI, and the diffusion of fluorescent muscimol was monitored under epifluorescence (Figure S7A). As expected by the topography of the V1-to-RL projection, selectively silencing caudal V1 reduced upper field responses in rostral RL (Figure 9G; medians: 3.8 versus 2.4 Hz; Wilcoxon rank-sum test; $p < 0.001$), whereas lower field responses were not affected (3.1 versus 3.1 Hz; Wilcoxon rank sum test; $p = 0.82$). Because we used vertical electrode arrays that spanned the entire cortical thickness, we analyzed whether the reduction of visual responsiveness observed after V1 silencing was different in the putative supragranular and infragranular layers in RL, but we failed to observe any difference (Figure S7B). These data suggest that retinotopically organized projections from V1 to RL are a determinant of visual responsiveness of RL and hence also of its multimodal character.

DISCUSSION

We made four main findings concerning MI in the mouse visuotactile area RL. (1) ME is more pronounced at the level of spike outputs compared to synaptic inputs; (2) ME is pronounced in supragranular pyramids but scarce among the deep infragranular pyramids and in the main interneuron population—Pv-INs; (3) the scarce ME of Pv-INs permits ME in neighboring pyramids; (4) there is a precise spatial distribution of uni- and bimodal cells at the microscale level.

Different Multisensory Integration of Synaptic Inputs and Spike Outputs

Whole-cell recordings combined with anatomical tracings suggest that RL neurons receive tactile and visual synaptic inputs from S1 and V1, respectively. However, fewer neurons in RL were bimodal al the level of APs than PSPs, and ME was stronger for APs compared to PSPs. This difference is presumably due to the nonlinear threshold mechanism underlying AP generation (see also Allman and Meredith, 2007; Schroeder and Foxe, 2002). The same threshold mechanism may account for the sublinear summation of PSPs on one hand, and for the (supra) linear summation of APs on the other hand.

The multisensory synaptic integration we observed in RL differs from the integration of two different *unisensory* stimuli in primary cortices. In primary cortices concurrent presentation of two unisensory stimuli typically *suppresses* responses, both in S1 (Higley and Contreras, 2005) and V1 (Priebe and Ferster, 2006), whereas in RL the interaction was largely additive. Interestingly, a similar difference between unimodal integration (suppression) and bimodal integration (enhancement) has been described in the cat colliculus (Alvarado et al., 2007). It would be interesting to investigate whether different cellular circuitries are responsible for these distinct computations.

Origin of the Scarce Multisensory Integration in Layer 5

While bimodal cells were more abundant in layer 5 compared to layer 2/3, ME was scarce in layer 5 pyramids, already for synaptic inputs. However, layer 5 is innervated by layer 2/3 neurons (Thomson and Bannister, 1998), and ME was common in the AP output of layer 2/3 pyramids. Why then do the two cortical layers have different ME, given this connection? A number of mechanisms can be hypothesized. First, many layer 5 cells do not receive inputs from layer 2/3 (Thomson and Bannister, 1998) but instead receive inputs from the thalamus (Ferster and Lindström, 1983) and layer 4 (Feldmeyer et al., 2005). Second, temporal integration properties in the cortex are layer specific. For example, the lower expression of HCN channels in layer 2/3 compared with layer 5 pyramids (Spruston, 2008) could enable stronger ME in layer 2/3, because HCN currents reduce temporal integration (Williams and Stuart, 2000). Third, the membrane potential of layer 5 pyramids is closer to AP threshold compared to supragranular pyramids (Medini, 2011) and layer 5 thick-tufted pyramids typically fire APs in bursts (de Kock et al., 2007). Thus, layer 5 pyramids could have a smaller margin to further increase responsiveness upon M stimulation compared to unimodal stimulation. Finally, regardless of the layer 2/3-to-5 projection, the possibility cannot be excluded that infragranular neurons could display ME in response to more complex or ecologically relevant stimuli.

Functional Significance of the Scarce Multisensory Enhancement in Pv-INs

ME was scarcer and less common in Pv-INs than in pyramids. This could be due to the fact that AP responses of Pv-INs are

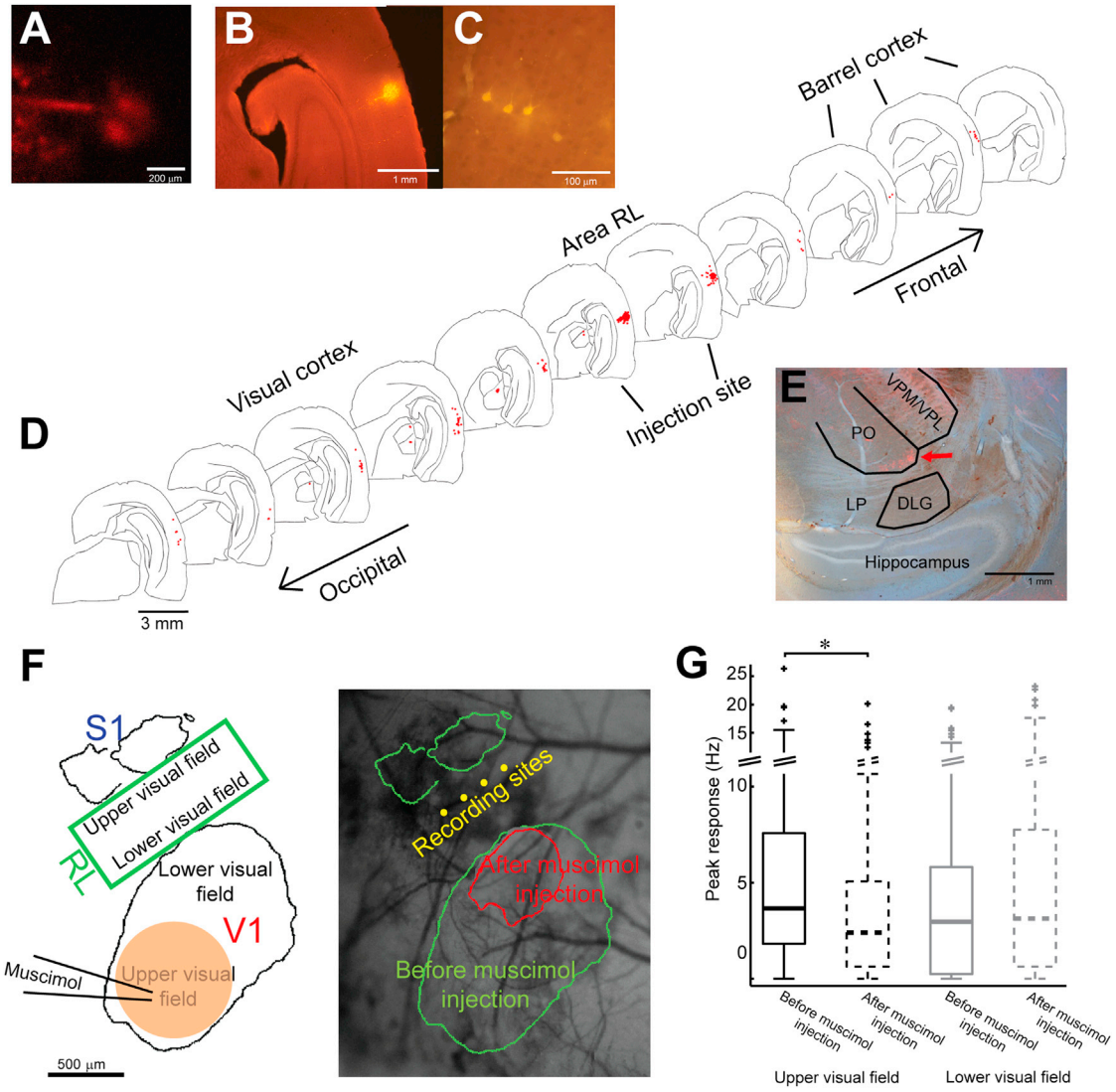

Figure 9. Anatomical and Functional Connectivity of Area RL

(A) Spread of the fluorescent tracer TMR-DA, visualized during the injection by a two-photon microscope (10× objective). The injection spot diameter was smaller than 300 μm.

(B) Extension of the injection site on a coronal brain section.

(C) Retrogradely labeled neurons in V1.

(D) Reconstructed serial coronal sections showing the injection site, and retrogradely labeled neurons (red asterisks). Every other section is shown and the remaining, intermediate sections were labeled for CO to identify layer 4 in V1 and S1 (and hence RL, see Figure 1C). Section thickness was 80 μm. The image shows sparse retrograde labeling in V1 and S1, and in the associative thalamic nucleus PO.

(E) Coronal section showing retrograde labeling (red arrow) in PO nucleus, but not in the specific visual and somatosensory nuclei (DLG and VPM-VPL, respectively; LP is the lateral posterior nucleus).

(F) Left: IOI was performed to locate V1, the α and β barrels in S1 (black), and area RL (green). Note the mirroring of the cortical representations of the upper and lower visual fields at the V1-RL border. Muscimol injections were targeted in caudal V1 by IOI (orange spot). Right: IOI was performed to locate the injection site and—after the injection—to determine the spatial extent of V1 silencing (red). Extracellular activity was recorded in the rostral RL (yellow dots), retinotopically corresponding to the silenced part of V1.

(G) AP responses to stimulation of the upper (black) and lower (gray) visual fields recorded in rostral RL before and after muscimol injection in caudal V1 (solid and dashed, respectively). Muscimol in caudal V1 selectively reduced upper visual field responses ($p < 0.05$).

See also Figure S7.

less sensitive to an increase in the strength of synaptic inputs compared to pyramids (Tateno et al., 2004). The weaker ME of Pv-INs could originate during the conversion of PSPs into APs. However, we did not record subthreshold activity from Pv-INs, so MI might be already weaker at the subthreshold level. In fact, Pv-INs have briefer excitatory currents and shorter EPSPs

that integrate less strongly over time compared to pyramids (Angulo et al., 1999; Thomson, 1997).

The results of our optogenetic manipulation of Pv-INs show that these inhibitory cells play a permissive role in the MI of pyramidal cells, because the *lack* of ME in Pv-INs enables the pyramidal cells to effectively integrate the inputs of different sensory modalities. Indeed, when we optogenetically induced an "artificial" ME at least in a subgroup of Pv-INs, we selectively disrupted ME in neighboring pyramids. Albeit what *causes* ME in pyramids is the concurrent arrival of two distinct sensory inputs in pyramidal cells that have intrinsic integration capabilities, our data indicate that the lack of integration in Pv-INs is a necessary condition enabling ME in pyramids.

One mechanism that could explain why photostimulation only promoted ME in a subgroup of Pv-INs is that adding some extra (photo)excitation during both uni- and multisensory stimulation might selectively favor M responses in those inhibitory cells with slightly more hyperpolarized membrane potentials. In these cases multisensory stimuli might elicit PSP responses significantly closer to the AP threshold than unisensory ones, and therefore promote higher ME.

These results suggest that the integrative properties of the major class of interneurons are important in enabling ME in excitatory cells. Other interneuron subtypes integrate inputs in different ways, and thus may differentially modulate MI in the excitatory cortical network. For example, recent work showed that somatostatin-positive inhibitory cells are effective integrators of sensory-driven synaptic inputs in V1 (Adesnik et al., 2012), contrasting with our results for Pv-INs in RL.

It is also interesting to compare our data on Pv-INs with the results obtained with optogenetic manipulation of Pv-INs in primary sensory cortices. In V1, neuronal responses to visual stimuli of different strengths (such as preferred or nonpreferred orientations) are all proportionately reduced by photoactivation of Pv-INs (Atallah et al., 2012; Wilson et al., 2012—but see Lee et al., 2012). In contrast, we did not observe such a linear/divisive effect of Pv-IN photostimulation on pyramids in RL. Rather than providing a divisive effect equally on all synaptic inputs, Pv-INs in RL provide a modulation akin to nonlinear normalization, in which stronger synaptic responses are inhibited more than weaker ones.

The larger impact of the photostimulation of Pv-INs on multisensory responses is probably due to the combined effect of different phenomena. First, our data show that the same degree of photostimulation increases more the spiking of Pv-INs during M stimulation than during unisensory stimulation (see Figure 8A). Second, synaptic connections between Pv-INs and pyramids are highly divergent (Helmstaedter et al., 2009). Thus, an increase in the percentage of Pv-INs showing ME during photostimulation might be enough to affect MI in pyramids. Third, the impact of inhibition might be larger on EPSPs of bigger amplitude (and thus on M responses), because the driving force for inhibition is larger during stronger depolarizations.

From the Spatial Structure of Microcircuits to Local and Long-Range Connectivity

The higher density of unimodal neurons near the borders of the primary cortices and the results of our retrograde tracings suggest a role for corticocortical connectivity in driving multimodal responses in RL (see also Wallace et al., 2004). We provided evidence that retinotopically organized corticocortical communication between V1 and RL is important for visual responsiveness in RL and hence, for its multisensory character as well. However, visual responses were not completely suppressed by local V1 inactivation, suggesting that the thalamic nucleus PO might convey some residual visual responses. Overall, our experiments suggest a combination of corticocortical and thalamocortical influences in shaping responses in RL. The anatomical connectivity pattern we found is not consistent with studies showing a predominant thalamic innervation of the rat posterior parietal cortex (Torrealba and Valdés, 2008) and of a parietotemporal auditory-tactile area (Brett-Green et al., 2003). Future experiments will clarify whether there is a common connectivity pattern for the multisensory cortices located between primary areas in rodents (Wallace et al., 2004).

We found that clusters of unimodal neurons are embedded into a matrix of bimodal neurons. Is this functional clustering unique to this area or is it a general cortical feature? This issue remains controversial in primary areas, also because there might be area-specific differences. There is evidence for functional microclustering of neurons according to the directional preference in rodent S1 (Kremer et al., 2011), but neurons in rodent V1 do not cluster according to their functional response properties, such as binocularity (Mrsic-Flogel et al., 2007) or orientation selectivity (Ohki et al., 2005). It will be interesting to investigate whether the microclustering we found is a feature of other association cortices in rodents.

Are the unimodal cells we identified with calcium imaging in RL functionally distinct from those of primary areas, or is RL a transition area where unimodal "primary" visual and tactile neurons, possibly left over during cortical area parcellation, coexist? The latter possibility seems unlikely for several reasons. First, many neurons that appear unimodal at suprathreshold level receive synaptic inputs from the other sensory modality, accounting for the fact that they also show ME (see Figure S3), as also described in cats (Allman and Meredith, 2007). Second, in primary cortices heteromodal inputs mostly give rise to inhibitory responses (Iurilli et al., 2012), that we failed to observe in RL. Third, we failed to find consistent labeling of specific thalamic nuclei (such as LGN or VPM) in our retrograde tracing studies, suggesting that unimodal neurons in RL have a distinct connectivity compared to unimodal neurons in primary cortices.

Multisensory Responses in a Mouse Parietal Association Cortex: Relation to Behavior

The functional responses of RL neurons appear to obey the "empirical principles of multisensory integration" (Stein and Stanford, 2008) such as evidence of significant ME, topographic alignment of the modality maps, and also adherence to the so-called "inverse effectiveness principle," in which a tactile stimulus preferentially enhances responses to weak rather than strong visual stimuli (e.g., non-preferred versus preferred direction of motion). This is line with the idea that one of the advantages of multisensory integration is to preferentially enhance sensory processing of weak or ambiguous sensory stimuli.

The multisensory character of RL has interesting implications with regard to its possible behavioral role. It has been recently proposed that the visual association areas that surround V1 might be involved in different types of visual processing. Area RL could belong to the more "dorsal" stream involved in visual motion coding, as suggested by the presence of many direction-selective neurons in RL (Marshel et al., 2011). Our data indicate that this view could be reconsidered, because RL has a clear multisensory (visuotactile) character, and because the visual direction selectivity could be disrupted by the arrival of a tactile stimulus (i.e., a given tactile stimulus preferentially enhances the visual response to the non-preferred direction compared to the preferred direction).

In this view, area RL is part of a circuit within the posterior parietal cortex of rodents that integrates visuotactile inputs in a behaviorally-relevant manner (Pinto-Hamuy et al., 1987). Area RL sends projections to motor areas related to whisker and eye movements (Wang et al., 2012). Also, area RL projects to other posterior parietal areas that are involved in path integration and spatial navigation, as shown by lesion (Whitlock et al., 2008) and imaging (Harvey et al., 2012) studies. Thus, it is plausible that RL integrates visual and tactile motion information to build a supramodal, egocentric spatial frame of reference useful for navigational behavior (Nitz, 2006; Whitlock et al., 2012).

Finally, our findings on multisensory processing might also have interesting implications for sensory plasticity, especially following sensory loss. We found that many neurons that appeared unimodal at AP level actually receive subthreshold inputs also from the other modality. This could provide a subthreshold "reservoir" for the expansion of the representation of the remaining sensory modalities that occurs as a consequence of complete sensory deprivations. This plastic reservoir is a potential target for alleviating sensory loss in pathological conditions.

EXPERIMENTAL PROCEDURES

All animal procedures were performed following EU and Italian Ministry of Health regulations on animal welfare and were oversighted by the Institutional Review Board. Mice were anesthetized with urethane (0.8–1.0 g/kg i.p.) and IOI was done to identify RL. Extracellular multiunit recordings were done with microelectrode arrays connected to a 16-channel system and spike sorting was done with principal components analysis. Population calcium imaging was done by pressure injection of OGB-1 AM under a two-photon system so to calculate the relative fluorescence (dF/F0) traces for single neurons. For whole-cell recordings, PSP and AP responses were measured upon averaging. For two-photon-targeted juxtasomal recordings of Pv-INs, we employed parvalbumin-Cre (PV-Cre) mice crossed to a Cre-responsive reporter line (Ai9-lsl-tdTomato), and extracellular pipettes filled with 25 μM Alexa-Fluor 488. The amplitude of averaged PSP and AP responses was compared with respect to baseline when the signal exceeded baseline + 3 SD. For the optogenetic modulation of Pv-INs, we crossed PV-Cre mice with a Cre-responsive reporter ChR2 line (*Ai27D (Rosa-CAG-LSL-hChR2(H134R)-tdTomato-WPRE*) (Madisen et al., 2012). Optic fiber photoactivation (491 nm; 105 μm inner core, 0.22 NA; 7 mW) lasted 500 ms and started 10 ms after the onset of sensory responses. Labeling of afferents to RL was done by injecting TMR-DA (3 kDa) in RL under a two-photon microscope. 0.5–1 μl of 10 mM fluorescent muscimol was injected in caudal V1 via IOI to block its activity. In all Figures, box plots represent the median, the 25th and 75th percentiles in the boxes, whereas the side bars represnt the 5th and 95th percentiles of the distribution. For statistical procedures and detailed information, see Supplemental Information.

SUPPLEMENTAL INFORMATION

Supplemental Information includes seven figures, four tables, Supplemental Experimental Procedures, and Supplemental Text and can be found with this article online at http://dx.doi.org/10.1016/j.neuron.2013.06.010.

ACKNOWLEDGMENTS

We thank John Assad and Tommaso Fellin for critically reading the manuscript, Marco Dal Maschio, Giacomo Pruzzo, and Mattia Pesce for technical assistance, Fabio Benfenati for departmental support, and Bojana Kokinovic for some histology.

Accepted: May 28, 2013
Published: July 11, 2013

REFERENCES

Adesnik, H., Bruns, W., Taniguchi, H., Huang, Z.J., and Scanziani, M. (2012). A neural circuit for spatial summation in visual cortex. Nature *490*, 226–231.

Allman, B.L., and Meredith, M.A. (2007). Multisensory processing in "unimodal" neurons: cross-modal subthreshold auditory effects in cat extrastriate visual cortex. J. Neurophysiol. *98*, 545–549.

Alvarado, J.C., Vaughan, J.W., Stanford, T.R., and Stein, B.E. (2007). Multisensory versus unisensory integration: contrasting modes in the superior colliculus. J. Neurophysiol. *97*, 3193–3205.

Andermann, M.L., Kerlin, A.M., Roumis, D.K., Glickfeld, L.L., and Reid, R.C. (2011). Functional specialization of mouse higher visual cortical areas. Neuron *72*, 1025–1039.

Angulo, M.C., Rossier, J., and Audinat, E. (1999). Postsynaptic glutamate receptors and integrative properties of fast-spiking interneurons in the rat neocortex. J. Neurophysiol. *82*, 1295–1302.

Atallah, B.V., Bruns, W., Carandini, M., and Scanziani, M. (2012). Parvalbumin-expressing interneurons linearly transform cortical responses to visual stimuli. Neuron *73*, 159–170.

Brett-Green, B., Fifková, E., Larue, D.T., Winer, J.A., and Barth, D.S. (2003). A multisensory zone in rat parietotemporal cortex: intra- and extracellular physiology and thalamocortical connections. J. Comp. Neurol. *460*, 223–237.

de Kock, C.P., Bruno, R.M., Spors, H., and Sakmann, B. (2007). Layer- and cell-type-specific suprathreshold stimulus representation in rat primary somatosensory cortex. J. Physiol. *581*, 139–154.

Dehner, L.R., Keniston, L.P., Clemo, H.R., and Meredith, M.A. (2004). Cross-modal circuitry between auditory and somatosensory areas of the cat anterior ectosylvian sulcal cortex: a 'new' inhibitory form of multisensory convergence. Cereb. Cortex *14*, 387–403.

Feldmeyer, D., Roth, A., and Sakmann, B. (2005). Monosynaptic connections between pairs of spiny stellate cells in layer 4 and pyramidal cells in layer 5A indicate that lemniscal and paralemniscal afferent pathways converge in the infragranular somatosensory cortex. J. Neurosci. *25*, 3423–3431.

Ferster, D., and Lindström, S. (1983). An intracellular analysis of geniculo-cortical connectivity in area 17 of the cat. J. Physiol. *342*, 181–215.

Foxworthy, W.A., Clemo, H.R., and Meredith, M.A. (2013). Laminar and connectional organization of a multisensory cortex. J. Comp. Neurol. *521*, 1867–1890.

Gentet, L.J., Avermann, M., Matyas, F., Staiger, J.F., and Petersen, C.C. (2010). Membrane potential dynamics of GABAergic neurons in the barrel cortex of behaving mice. Neuron *65*, 422–435.

Gentet, L.J., Kremer, Y., Taniguchi, H., Huang, Z.J., Staiger, J.F., and Petersen, C.C. (2012). Unique functional properties of somatostatin-expressing GABAergic neurons in mouse barrel cortex. Nat. Neurosci. *15*, 607–612.

Harvey, C.D., Coen, P., and Tank, D.W. (2012). Choice-specific sequences in parietal cortex during a virtual-navigation decision task. Nature *484*, 62–68.

Helmstaedter, M., Sakmann, B., and Feldmeyer, D. (2009). Neuronal correlates of local, lateral, and translaminar inhibition with reference to cortical columns. Cereb. Cortex *19*, 926–937.

Higley, M.J., and Contreras, D. (2005). Integration of synaptic responses to neighboring whiskers in rat barrel cortex in vivo. J. Neurophysiol. *93*, 1920–1934.

Iurilli, G., Ghezzi, D., Olcese, U., Lassi, G., Nazzaro, C., Tonini, R., Tucci, V., Benfenati, F., and Medini, P. (2012). Sound-driven synaptic inhibition in primary visual cortex. Neuron *73*, 814–828.

Jiang, W., Wallace, M.T., Jiang, H., Vaughan, J.W., and Stein, B.E. (2001). Two cortical areas mediate multisensory integration in superior colliculus neurons. J. Neurophysiol. *85*, 506–522.

Kameyama, K., Sohya, K., Ebina, T., Fukuda, A., Yanagawa, Y., and Tsumoto, T. (2010). Difference in binocularity and ocular dominance plasticity between GABAergic and excitatory cortical neurons. J. Neurosci. *30*, 1551–1559.

Kerlin, A.M., Andermann, M.L., Berezovskii, V.K., and Reid, R.C. (2010). Broadly tuned response properties of diverse inhibitory neuron subtypes in mouse visual cortex. Neuron *67*, 858–871.

Komiyama, T., Sato, T.R., O'Connor, D.H., Zhang, Y.X., Huber, D., Hooks, B.M., Gabitto, M., and Svoboda, K. (2010). Learning-related fine-scale specificity imaged in motor cortex circuits of behaving mice. Nature *464*, 1182–1186.

Kremer, Y., Léger, J.F., Goodman, D., Brette, R., and Bourdieu, L. (2011). Late emergence of the vibrissa direction selectivity map in the rat barrel cortex. J. Neurosci. *31*, 10689–10700.

Lee, S.H., Kwan, A.C., Zhang, S., Phoumthipphavong, V., Flannery, J.G., Masmanidis, S.C., Taniguchi, H., Huang, Z.J., Zhang, F., Boyden, E.S., et al. (2012). Activation of specific interneurons improves V1 feature selectivity and visual perception. Nature *488*, 379–383.

Madisen, L., Mao, T., Koch, H., Zhuo, J.M., Berenyi, A., Fujisawa, S., Hsu, Y.W., Garcia, A.J., 3rd, Gu, X., Zanella, S., et al. (2012). A toolbox of Cre-dependent optogenetic transgenic mice for light-induced activation and silencing. Nat. Neurosci. *15*, 793–802.

Marshel, J.H., Garrett, M.E., Nauhaus, I., and Callaway, E.M. (2011). Functional specialization of seven mouse visual cortical areas. Neuron *72*, 1040–1054.

Martinez, L.M., Wang, Q., Reid, R.C., Pillai, C., Alonso, J.M., Sommer, F.T., and Hirsch, J.A. (2005). Receptive field structure varies with layer in the primary visual cortex. Nat. Neurosci. *8*, 372–379.

Medini, P. (2011). Layer- and cell-type-specific subthreshold and suprathreshold effects of long-term monocular deprivation in rat visual cortex. J. Neurosci. *31*, 17134–17148.

Mrsic-Flogel, T.D., Hofer, S.B., Ohki, K., Reid, R.C., Bonhoeffer, T., and Hübener, M. (2007). Homeostatic regulation of eye-specific responses in visual cortex during ocular dominance plasticity. Neuron *54*, 961–972.

Nitz, D.A. (2006). Tracking route progression in the posterior parietal cortex. Neuron *49*, 747–756.

Ohki, K., Chung, S., Ch'ng, Y.H., Kara, P., and Reid, R.C. (2005). Functional imaging with cellular resolution reveals precise micro-architecture in visual cortex. Nature *433*, 597–603.

Pinto-Hamuy, T., Olavarria, J., Guic-Robles, E., Morgues, M., Nassal, O., and Petit, D. (1987). Rats with lesions in anteromedial extrastriate cortex fail to learn a visuosomatic conditional response. Behav. Brain Res. *25*, 221–231.

Priebe, N.J., and Ferster, D. (2006). Mechanisms underlying cross-orientation suppression in cat visual cortex. Nat. Neurosci. *9*, 552–561.

Roth, M.M., Helmchen, F., and Kampa, B.M. (2012). Distinct functional properties of primary and posteromedial visual area of mouse neocortex. J. Neurosci. *32*, 9716–9726.

Runyan, C.A., Schummers, J., Van Wart, A., Kuhlman, S.J., Wilson, N.R., Huang, Z.J., and Sur, M. (2010). Response features of parvalbumin-expressing interneurons suggest precise roles for subtypes of inhibition in visual cortex. Neuron *67*, 847–857.

Sakata, S., and Harris, K.D. (2009). Laminar structure of spontaneous and sensory-evoked population activity in auditory cortex. Neuron *64*, 404–418.

Schroeder, C.E., and Foxe, J.J. (2002). The timing and laminar profile of converging inputs to multisensory areas of the macaque neocortex. Brain Res. Cogn. Brain Res. *14*, 187–198.

Spruston, N. (2008). Pyramidal neurons: dendritic structure and synaptic integration. Nat. Rev. Neurosci. *9*, 206–221.

Stein, B.E., and Stanford, T.R. (2008). Multisensory integration: current issues from the perspective of the single neuron. Nat. Rev. Neurosci. *9*, 255–266.

Stein, B.E., and Wallace, M.T. (1996). Comparisons of cross-modality integration in midbrain and cortex. Prog. Brain Res. *112*, 289–299.

Tateno, T., Harsch, A., and Robinson, H.P. (2004). Threshold firing frequency-current relationships of neurons in rat somatosensory cortex: type 1 and type 2 dynamics. J. Neurophysiol. *92*, 2283–2294.

Thomson, A.M. (1997). Activity-dependent properties of synaptic transmission at two classes of connections made by rat neocortical pyramidal axons in vitro. J. Physiol. *502*, 131–147.

Thomson, A.M., and Bannister, A.P. (1998). Postsynaptic pyramidal target selection by descending layer III pyramidal axons: dual intracellular recordings and biocytin filling in slices of rat neocortex. Neuroscience *84*, 669–683.

Torrealba, F., and Valdés, J.L. (2008). The parietal association cortex of the rat. Biol. Res. *41*, 369–377.

Wallace, M.T., Ramachandran, R., and Stein, B.E. (2004). A revised view of sensory cortical parcellation. Proc. Natl. Acad. Sci. USA *101*, 2167–2172.

Wang, Q., and Burkhalter, A. (2007). Area map of mouse visual cortex. J. Comp. Neurol. *502*, 339–357.

Wang, Q., Sporns, O., and Burkhalter, A. (2012). Network analysis of corticocortical connections reveals ventral and dorsal processing streams in mouse visual cortex. J. Neurosci. *32*, 4386–4399.

Whitlock, J.R., Sutherland, R.J., Witter, M.P., Moser, M.B., and Moser, E.I. (2008). Navigating from hippocampus to parietal cortex. Proc. Natl. Acad. Sci. USA *105*, 14755–14762.

Whitlock, J.R., Pfuhl, G., Dagslott, N., Moser, M.B., and Moser, E.I. (2012). Functional split between parietal and entorhinal cortices in the rat. Neuron *73*, 789–802.

Williams, S.R., and Stuart, G.J. (2000). Site independence of EPSP time course is mediated by dendritic I(h) in neocortical pyramidal neurons. J. Neurophysiol. *83*, 3177–3182.

Wilson, N.R., Runyan, C.A., Wang, F.L., and Sur, M. (2012). Division and subtraction by distinct cortical inhibitory networks in vivo. Nature *488*, 343–348.